First-Principles Dynamics along the Reaction Path of $CH_3CH_2 + O_2 \rightarrow H_2C{=}CH_2 + HOO$: Evidence for Vibronic State Mixing and Neutral Hydrogen Transfer†

Amity Andersen and Emily A. Carter*

Department of Chemistry and Biochemistry, University of California, Los Angeles, Box 951569, Los Angeles, California 90095-1569

We employ Born−Oppenheimer molecular dynamics (BOMD), with forces derived from spin-polarized density functional theory using the B3LYP hybrid exchange-correlation functional, to explore the dynamics of oxidation of ethyl radical to produce ethylene, along the concerted-elimination path $CH_3CH_2 + O_2 \rightarrow CH_3CH_2OO \rightarrow CH_2{=}CH_2 + HOO$. The transition state connecting CH_3CH_2OO to $CH_2{=}CH_2$ and HOO has a planar, five-membered-ring structure ···C−C−H−O−O··· known as TS1. The electronic nature of this saddle point has been the subject of controversy. Recent *ab initio* calculations have indicated that TS1 has a $^2A''$ electronic ground state within C_s symmetry. In this state, intramolecular neutral hydrogen transfer from the methyl group of the intermediate ethylperoxy radical ($CH_3CH_2OO\cdot$) to the terminal oxygen is hindered by the lack of overlap between the 1s orbital of the in-plane hydrogen atom and the singly-occupied 2p (a″) orbital of the terminal oxygen. Previous explanations invoked proton transfer, a rather unpalatable process for an alkylperoxy radical. Two other possibilities that both facilitate neutral H-transfer are explored in the present work, namely: (i) an O_2 π^*-resonance mechanism and (ii) $^2A'-{}^2A''$ state mixing. First, we show that the structure of TS1 is a "late," loose transition state, consistent with a loosely coupled O_2 that can shift π^*-electrons to aid neutral hydrogen atom transfer. Second, our BOMD trajectories reveal that torsional motion in the ethylperoxy radical and at the transition state causes symmetry-breaking and $^2A'-{}^2A''$ state mixing. The low-lying $^2A'$ excited state, with its in-plane, singly occupied oxygen 2p orbital, can easily transfer a neutral H atom. Not only is vibrationally-induced symmetry-breaking present near (and after crossing) TS1, but also in the CH_3CH_2 and O_2 entrance channel, which again exhibits torsional motion that allows both the $^2A''$ ground state and the excited $^2A'$ state to be accessed while forming the ethylperoxy radical. Thus we propose that vibronic state mixing is a key feature of the reaction dynamics of ethane combustion, helping to facilitate dehydrogenation.

I. Introduction

In the oxidation processes of many organic compounds, organic peroxy radicals are key intermediates. In the atmosphere, organic peroxy radicals react with NO to form NO_2 which can be photolyzed to form ground-state $O(^3P)$, a precursor in the production of tropospheric ozone.[1,2,3,4] Peroxy radicals play a major role in autoignition which is responsible for "knock", the undesirable sound made by the spontaneous ignition in internal combustion engines, which can be damaging to engine components.[5] Fuel efficiency, however, increases with a fuel's ability to compression ignite.[5] Therefore, a detailed knowledge of the mechanisms involving these important intermediates is vital to optimizing fuels used in internal combustion engines to maximize fuel efficiency and economy and minimize "knock"[5] and to establishing environmental controls and policies.[1−4,6]

Reactivity of a general peroxy radical, ROO·, depends on the properties of the R· moiety.[1,3,5] Studies on the oxidation of simple alkanes may provide insight into the oxidation of larger, more complex molecules present in internal combustion engines and in the atmosphere. In particular, ethane oxidation produces the smallest alkyl peroxy radical (ethylperoxy) intermediate with the structural flexibility to undergo intramolecular isomerization.[7] Thus, ethane oxidation serves as a prototype reaction for larger and more complex alkanes (and possibly other organic compounds). Introduced by Semenov,[8] the accepted mechanism for ethane oxidation (and alkane oxidation in general) is a chain-reaction mechanism starting with an "initiation" step followed by "propagation", "branching", and finally "termination". Ethane oxidation is initiated by the removal of a hydrogen atom from ethane by a highly reactive radical present in the system (typically hydroxyl radical in the atmosphere or halogen atoms in a laboratory setting) to form an alkyl radical. The propagation steps following this initiation step involve the reaction of molecular oxygen with an ethyl radical. What happens next has enjoyed a long and controversial history which has been discussed extensively in the recent theoretical works of Schaefer and co-workers.[9−12] Here, we only consider the possible propagation mechanisms of ethane oxidation, and of these possible mechanisms, we have considered only a small subset, the ethylene-producing mechanisms, which will be discussed shortly.

The most recent of these studies from the Schaefer group, Ignatyev et al.,[11] and Rienstra-Kiracofe et al.[12] represent the "best" mapping to date of the potential energy surface (PES) describing the possible reaction mechanisms in ethane oxidation starting with ethyl radical and molecular oxygen (the reactants in the chain-reaction propagation step of ethane oxidation). In these complementary studies, Ignatyev et al.[11] and Rienstra-Kiracofe et al.[12] have applied density functional theory (DFT) and coupled-cluster single and double with perturbative triple excitations (CCSD(T)) theory, respectively. Both theoretical

† Part of the special issue "Jack Beauchamp Festschrift". We are happy to dedicate this paper in honor of Jack Beauchamp, a dear friend and colleague, and gas phase ion chemist extraordinaire.

* Corresponding author. E-mail: eac@chem.ucla.edu.

10.1021/jp0206267 CCC: $22.00
Published on Web 09/18/2002

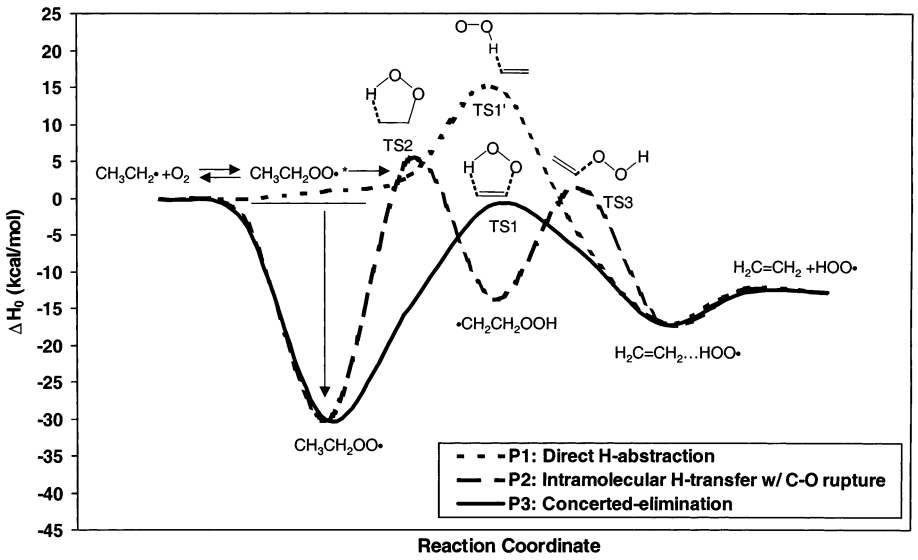

Figure 1. Three paths from ethyl radical and molecular oxygen to ethylene and hydroperoxy radical. Activation energies of transition states and the enthalpies (at 0 K) of stable species are taken from "the best" *ab initio* results of Rienstra-Kiracofe et al.[12]

studies consider three primary paths which start with the reactants (ethyl radical and molecular oxygen) and end with the products ethylene and hydroperoxy radical. In addition to the ethylene-producing paths, Rienstra-Kiracofe et al. described two possible paths leading to ethylene oxide and hydroxy radical and one leading to acetaldehyde and hydroxy radical. Figure 1 shows the PES's of the three ethylene-producing reaction paths according to the "best" *ab initio* calculations of Rienstra-Kiracofe et al.[12]

The first proposed path leading to the production of ethylene and hydroperoxy radical is the direct hydrogen atom abstraction path, with transition state, TS1′ (P1 in Figure 1):

$$O_2 + H{-}CH_2CH_2 \rightarrow TS1' \rightarrow OOH + CH_2{=}CH_2 \quad (1)$$

The two other paths operate through a Lindemann-type mechanism (P2 and P3 in Figure 1). Both paths begin with the addition of molecular oxygen to ethyl radical to form a vibrationally excited ethylperoxy complex:

$$CH_3CH_2 + O_2 \rightarrow CH_3CH_2OO^* \quad (2)$$

O_2 readily adds to ethyl radical. This reaction has been shown through ab initio calculations to be "barrierless".[11,12] Moreover, Knox and Norrish have observed a "negative temperature coefficient" between 648 and 708 K associated with this reaction;[13] the following steps have been proposed to explain this. The first of these is that ethylperoxy radical can dissociate back into ethyl radical and molecular oxygen:

$$CH_3CH_2 + O_2 \rightleftharpoons CH_3CH_2OO^* \quad (3)$$

or the vibrationally excited ethylperoxy radical can be collisionally stabilized:

$$CH_3CH_2OO^* + M \rightarrow CH_3CH_2OO + M \quad (4)$$

or can cross over a barrier (TS1 or TS2) to form other intermediates or products. The two paths (P2 and P3) that can be followed after the formation of the vibrationally-activated $CH_3CH_2OO^*$ are (i) isomerization via intramolecular hydrogen atom transfer and (ii) concerted-elimination of HO_2. The former path goes through an asymmetric, nonplanar, five-membered-ring transition state, TS2, and leads to a relatively stable hydroperoxyethyl radical which can subsequently dissociate into ethylene and hydroperoxy radical by crossing over a second transition state, TS3, (P2 in Figure 1).

$$CH_3CH_2OO^* \rightarrow TS2 \rightarrow CH_2CH_2OOH \rightarrow TS3 \rightarrow CH_2{=}CH_2 + HOO \quad (5)$$

The latter path involves concerted-elimination via a planar, five-membered-ring transition state, TS1, that dissociates directly into ethylene and hydroperoxy radical.

$$CH_3CH_2OO^* \rightarrow TS1 \rightarrow CH_2{=}CH_2 + HOO \quad (6)$$

Experimental observations[14−17] and kinetic modeling[18,19] support a Lindemann-type scheme for the low-temperature (<1000 K) production of ethylene and hydroperoxy radical. For example, Kaiser et al.[14,15] have shown in their smog chamber experiments that ethylene production decreases with increasing pressure for temperatures 264−529 K, indicative of collisional stabilization of the ethylperoxy radical. This evidence shows that the direct hydrogen abstraction path (P1) is irrelevant at low temperatures.

As for the other two paths (P2 and P3), Kaiser's experiments regarding the effects of temperature on ethylene yield,[17] combined with Schaefer and co-workers' calculations, lead one to conclude that the concerted-elimination channel through TS1 (P3) is the only means of producing ethylene and hydroperoxy radicals at temperatures lower than 400 K. An Arrhenius fit to the experimental data provides a 1.1 kcal/mol upper limit to the $CH_3CH_2OO^* \rightarrow CH_2{=}CH_2 + HOO$ "apparent" barrier (with respect to the energy of the reactants, ethyl radical, and O_2) for temperatures below 400 K. From Figure 1, one can see that the barrier for the concerted-elimination path (TS1) is the lowest barrier relative to the reactants. The best DFT (UB3LYP/TZ2P) calculations of Ignatyev et al.[11] and the best, high-quality ab initio (CCSD(T)/TZ2Pf//CCSD(T)/TZ2P) calculations of Rienstra-Kiracofe et al.[12] place the zero-point-corrected TS1 activation energy at 1.9 and 0.9 kcal/mol below the reactants, respectively; Ignatyev et al. and Rienstra-Kiracofe et al. report that the second highest barrier, the intramolecular H-transfer barrier (TS2), is 8.0 and 5.3 kcal/mol above the reactants, respectively. Though TS2 has a five-membered-ring structure like that of TS1, TS2 has a twisted structure with no symmetry.

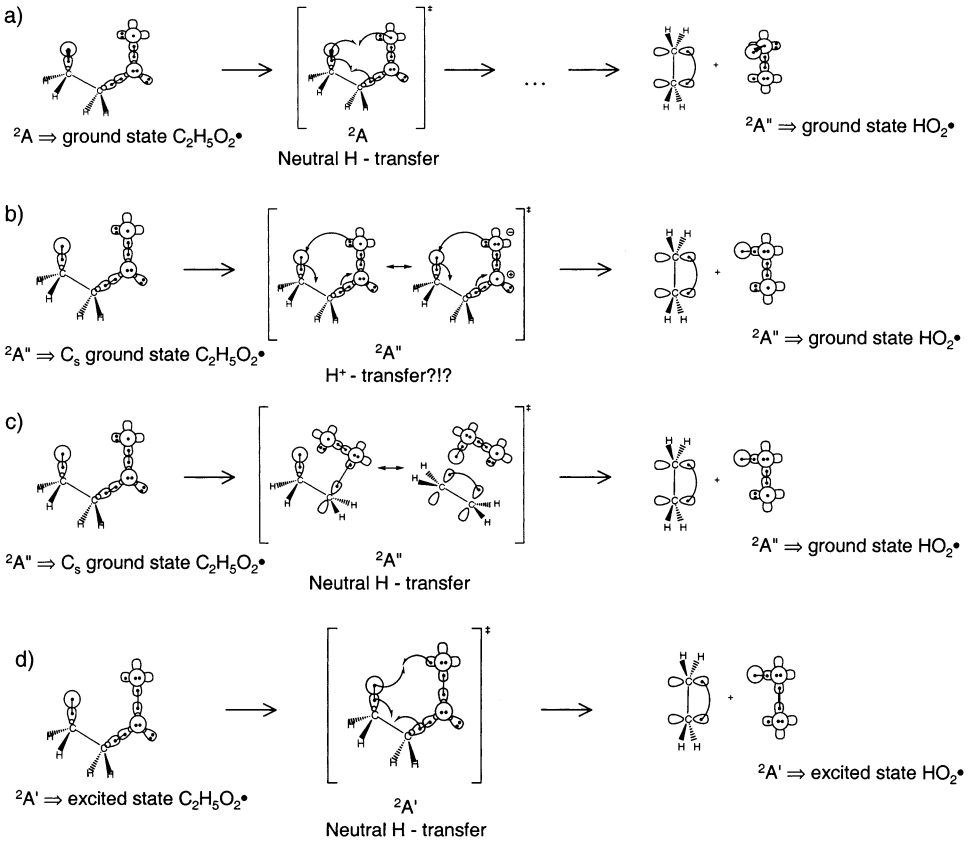

Figure 2. (a) Intramolecular hydrogen transfer via C−C rotation of in-plane methyl hydrogen out of plane. (b) Concerted intramolecular proton transfer. (c) Neutral H-transfer via π-resonance on O_2. For parts a−c, the HOO product is in the $\tilde{X}\,^2A''$ ground state. (d) Concerted-elimination of HOO on the $^2A'$ excited-state surface.

The structure of TS2 also has a more compact ring structure than that of TS1; for example, the C−O bond lengths, according to the best calculations of Ignatyev et al.[11] and Rienstra-Kiracofe et al.[12] are 2.138 and 2.194 Å, respectively, for TS1, and 1.436 and 1.431 Å, respectively, for TS2. Thus, ring strain may be responsible for TS2 having a higher energy than that of TS1. Finally, Ignatyev et al. and Rienstra-Kiracofe et al. reported that the barrier heights of the direct hydrogen abstraction (TS1′) are 10.2 and 15.1 kcal/mol (relative to the reactants), respectively. For temperatures in the range 400−529 K, the ethylene percent yield increases dramatically and Kaiser has reported an "apparent" barrier of about 25 kcal/mol with respect to CH_3CH_2 and O_2. Kaiser has proposed that the equilibrium of eq 3 will shift to the left with increasing temperature. Following the dissociation of CH_3CH_2OO back into CH_3CH_2 and O_2, CH_3-CH_2 and O_2 can recombine and continue to cycle through eq 3. This reflux mechanism would allow more opportunities to form ethylperoxy complexes with the right distribution of internal energy to overcome the TS1 activation barrier. Also, the ethylperoxy radical will be less stable at higher temperatures; therefore thermally-activated ethylperoxy radicals add to the pool of complexes that will readily pass over the TS1 barrier. With an "apparent" activation energy of about 25 kcal/mol, TS2 and TS1′ may be low enough to allow the P1 and P2 channels to compete with the P3 channel. Though it has been argued that the direct abstraction path (P1) is not important at temperatures below 1000 K,[3,7] Kaiser has shown that the pressure dependence of ethylene percent yield decreases gradually as the temperature is raised, which may indicate a small contribution from the direct hydrogen abstraction path. As we are interested in the most important channel in the low-temperature production of ethylene, we focus here only on P2 and P3.

Although TS1 meets the 1.1 kcal/mol upper limit to ethylene and hydroperoxy radical productions set by Kaiser for temperatures below 400 K, the predicted electronic ground state of TS1 is $^2A''$; this implies that the oxygen 2p orbital containing the unpaired electron is perpendicular to the mirror plane formed by the two oxygen atoms, the two carbon atoms, and the transferring hydrogen atom of the methyl group. This observation introduces a mechanistic dilemma which has been discussed thoroughly by Clifford et al.[20] in the course of their negative-ion photoelectron detachment of *tert*-butyl hydroperoxide study. If C_s symmetry and the electronic $^2A''$ ground state is assumed for TS1, they (as well as others before them[9,10,16]) noted that the singly occupied p-orbital on the terminal oxygen atom of the ethylperoxy complex involved in the intramolecular hydrogen transfer is perpendicular to the mirror plane and is orthogonal to the 1s orbital of the in-plane, methyl hydrogen atom. Rotating the transferring hydrogen out of plane via internal rotation along the C−C bond increases the overlap between the hydrogen atom's 1s orbital and the oxygen atom's half-occupied 2p orbital (see Figure 2a). This essentially gives the TS2 structure. Wagner et al.[16] (before the *ab initio* studies of Ignatyev et al.[11] and Rienstra-Kiracofe et al.[12]) assumed this puckered-ring structure and adopted the (P2) isomerization path (eq 5) in their RRKM/kinetics study. In the RRKM modeling of their data, they treated the energy of this puckered-ring transition-state structure as an adjustable parameter and variationally determined this parameter to have an enthalpy of −2.4 kcal/mol (at 0 K) with respect to CH_3CH_2 and O_2. This placement of the energy of TS2 below reactants is not supported by the

later *ab initio* studies of Schaefer and co-workers,[11,12] who found TS2 to be 5−8 kcal/mol above reactants. Interestingly, Wagner et al.[16] assumed that the section of the P2 path following this puckered-ring transition state was of negligible importance. By this, they meant that once the transition-state barrier was surmounted, the hydroperoxyethyl would immediately and irreversibly form ethylene and hydroperoxy radical. This was a reasonable assumption, since they used Benson's estimate[21] for the transition state from hydroperoxyethyl to the $CH_2{=}CH_2$ and HOO products (TS3), placed at 7.0 kcal/mol below CH_3CH_2 and O_2.

By contrast, the CH_2CH_2OOH radical has been argued by Walker and co-workers[22,23] to have a significant lifetime. From their reactor chamber kinetics studies on the reverse path (HOO addition to ethylene), Walker and co-workers[22−24] inferred that the hydroperoxyethyl radical produced by HOO addition to ethylene did not predominantly dissociate back into ethylene and HOO, but instead tended to produce ethylene oxide and hydroxyl radical. In modeling their kinetics data, they reported a 17 kcal/mol TS3 activation energy with respect to $CH_2{=}CH_2$ and HOO. This would put TS3 4 kcal/mol above ethyl radical and molecular oxygen and create a substantial bottleneck on the way to ethylene and hydroperoxy radical production. Hydroperoxyethyl radical accumulating before TS3 may then have the opportunity to be involved in secondary chemistry such as combining with another O_2 to create $OOCH_2CH_2OOH$ (an important radical in "branching", the combustion step leading to the explosive nature of combustion[7]), or forming ethylene oxide and hydroxyl radical[22] rather than decomposing solely into ethylene and hydroperoxy radical. Indeed, the *ab initio* studies of Ignatyev et al.[11] and Rienstra-Kiracofe et al.[12] put TS3 at 1.5 and 1.4 kcal/mol above the reactants, respectively. To account for this apparent inconsistency, Walker and co-workers[22] proposed the "concerted" path (P3) that bypasses the production of the hydroperoxyethyl radical in the production of ethylene and HOO.

This brings us back to P3 with transition state TS1 and the dilemma associated with transferring an in-plane methyl hydrogen to a terminal oxygen with no orbital overlap. One interpretation of the planar five-membered-ring transfer pathway that retains the C_s symmetry of the TS1 structure was proposed briefly by Ignatyev et al.[11] and elaborated upon by Clifford et al.:[20] an intramolecular "proton" transfer (see Figure 2b). The transition state consists of a mixture of the ground state, $\tilde{X}\,^2A''$, and the lowest-lying $\tilde{B}\,^2A''$ excited state, in which the excited $\tilde{B}\,^2A''$ configuration is able to facilitate the intramolecular proton transfer[20] (see Figure 2b). A proton-transfer rankles one's chemical intuition, however, given that an alkyl hydrogen is not expected to be very acidic (Table 2 of the review of Berkowitz et al.[25] places the acidity of methane, $\Delta_{acid}H_{298}(H_3C{-}H) = 416.7{\pm}0.7$ kcal/mol, as the only known alkane gas-phase acidity; larger-alkane gas-phase acidities have never been measured). Besides, Clifford et al. have estimated that this $\tilde{B}\,^2A''$ is 5 eV higher than the ground state,[20] which would imply that mixing is highly unlikely.

Another possible mechanism,[26] which would bypass the need for proton transfer, is shown in Figure 2c. In this situation, the ethyl radical and O_2 fragments are loosely associated with each other through long-range coupling between the resonating oxygen radical center and the carbon radical center. By allowing O_2 to have a near-isolated electronic structure, the in-plane, resonating oxygen π-electron can shift from oxygen center to oxygen center and therefore can be in a position to pair up with the in-plane hydrogen's electron. This argues for a "late," loose transition state. From ethylperoxy radical to ethylene and hydroperoxy radical, the reaction is endothermic by about 22 kcal/mol;[20,27] thus one expects Hammond's postulate to apply, wherein the TS1 transition complex is product-like in structure. Consistent with this idea, Rienstra-Kiracofe et al.[12] predicted (at the CCSD(T)/TZ2P level of theory) a C−O bond length for the TS1 complex of 2.138 Å (2.194 Å according to the UB3LYP/TZ2Pf calculations of Ignatyev et al.[11]), indicating that the C−O bond is extremely stretched. The transferring hydrogen atom is closer to the oxygen atom it is transferring to (1.259 Å[12] and 1.274 Å[11]) than it is to the carbon atom it came from (1.362 Å[12] and 1.352 Å[11]), but is indeed quite far away from both. The C−C bond length (1.392 Å[12] and 1.383 Å[11]) in the complex is closer in length to the C−C bond in ethylene (1.336 Å[12] and 1.325 Å[11]) than it is to the length of the C−C bond in ethylperoxy radical in the *gauche* conformation (1.522 Å[12] and 1.514 Å[11]). The O−O bond lengths in TS1 are 1.287 and 1.269 Å according to Rienstra-Kiracofe et al.[12] and Ignatyev et al.,[11] respectively, which is intermediate between the shorter bond in $^3\Sigma_g^-$ O_2 (1.220 Å according to Rienstra-Kiracofe et al.[12] and 1.206 Å according to Ignatyev et al.[11]) and the longer O−O bonds in HOO and ethylperoxy radical calculated by Rienstra-Kiracofe et al.[12] (1.350 and 1.344 Å, respectively) and Ignatyev et al.[11] (1.327 and 1.315 Å, respectively). The geometry of TS1 is therefore consistent with a fairly decoupled O_2, which would then allow neutral H-transfer to occur as suggested above.

Finally, the last possible mechanism we consider is that the ethylperoxy radical undergoing the transition to ethylene and hydroperoxy radical is not necessarily in the ground electronic state $\tilde{X}\,^2A''$, but rather it may be in the low-lying $\tilde{A}^2A'$ excited electronic state (see Figure 2d). Spectroscopists Hunziker and Wendt observed the lowest-lying $^2A'$ electronic state of CH_3-CH_2OO, reporting a $\tilde{A}\,^2A' \leftarrow \tilde{X}\,^2A''$ transition of 0.9414 ± 0.0008 eV (T_0).[28] Recent negative-ion photoelectron detachment experiments on $CH_3CH_2OO^-$ by Blanksby et al. confirmed this value (0.938 ± 0.004 eV).[27] Quelch et al.[9,10] discussed, through ab initio calculations at the DZP/CISD+Q level of theory, the possibility that the low-lying $^2A'$ state may be involved in ethane oxidation, since its formation is still exothermic with respect to reactants. They calculated the low-lying $^2A'$ excited state of ethylperoxy radical to be about 0.755 eV higher than the $^2A''$ ground state of ethylperoxy radical. They argued that this $^2A'$ excited-state correlates with a singlet $O_2(^1\Delta_g)$ reactant ($O_2(^1\Delta_g)$ is 0.9817 ± 0.0001 eV (T_e) higher than ground-state O_2-($^3\Sigma_g^-$)[29]). From a molecular orbital (MO) analysis, they proposed that a CH_3CH_2OO $\tilde{A}\,^2A' - \tilde{X}\,^2A''$ interaction could be possible. Figure 3 schematically depicts the correlation between excited $^1\Delta_g$ O_2 and the excited $^2A'$ ethylperoxy radical, as well as between $^3\Sigma_g^-$ O_2 and the ground-state $^2A''$ ethylperoxy radical. This same argument has been applied in Walch's theoretical work on an analogous (but highly strained) alkane system, $CH_3 + O_2$ addition.[30] Such transitions suggest the presence of conical intersections, which have been proposed by Pilling and co-workers[31,32] and elaborated on (with the addition of charge-transfer models) by Stark[33] to rationalize the discrepancies between the observations of Walker and co-workers and the work of Gutman and co-workers (mentioned above). Stark performed some preliminary UCIS/6-31G(d) calculations to search for an "unavoided crossing" along the C−O bond coordinate; from these calculations, he speculated that the intersection point between the $^2A''$ and $^2A'$ states is at a C−O distance of 2.6 Å. If Stark's preliminary calculations are right, an "unavoided crossing" point is located about 0.5 Å after TS1 on the PES along the C−O bond coordinate in close

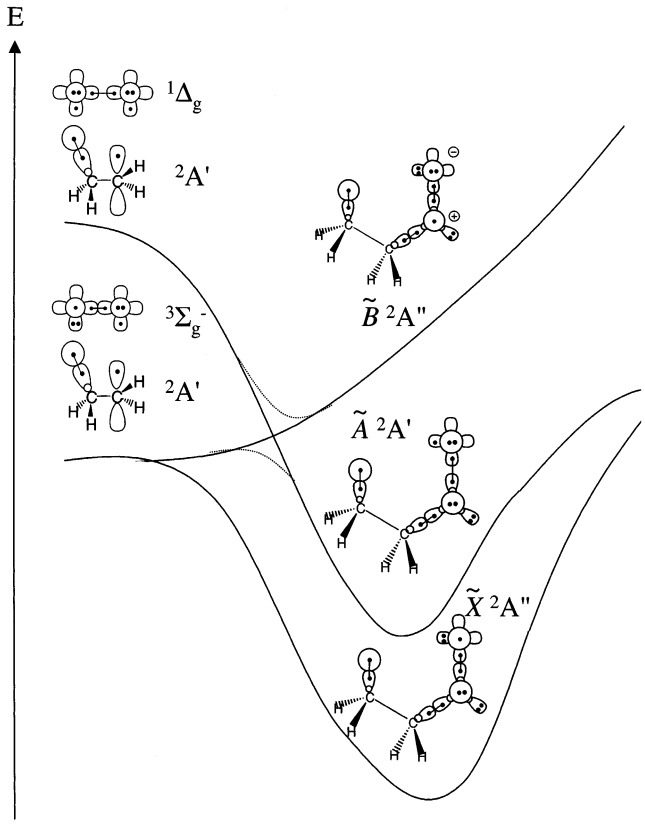

Figure 3. Schematic correlation diagram displaying crossings of low-lying PES's derived from ground-state $^3\Sigma_g^-$ O_2 + ^{2}A′ CH_3CH_2 → ^{2}A″ CH_3CH_2OO and excited state $^1\Delta_g$ O_2 + ^{2}Ã′ CH_3CH_2 → ^{2}A′ CH_3CH_2-OO. Note, for simplicity, only one resonance structure of O_2 is shown for each state.

proximity to TS1. While exploring the relative energies of the ^{2}A′ and ^{2}A″ states, Rienstra-Kiracofe et al.[12] found a ^{2}A′ transition state (TS2′), similar—but planar—in structure to the asymmetric TS2 (^{2}A) transition state, which was 14.9 kcal/mol higher in energy than TS2 (^{2}A) and 9.8 kcal/mol higher than the ^{2}A″ state constrained to the same structure as TS2′. Additionally, they found a ^{2}A′ excited state at the TS1 structure 44.2 kcal/mol above the ^{2}A″ ground state. Clifford et al.[20] have noted that experimental evidence for interconversion of $\tilde{A}\ ^2$A′ → $\tilde{X}\ ^2$A″ in ROO exists, at least for HOO.[34] Zabel et al.[34] detected near-IR chemiluminescence from HOO ($\tilde{X}\ ^2$A″, $\upsilon_3' \leq 6$; where υ_3' is the O—O stretch frequency) from thermal recombination of H and O_2 in a fast-flow reactor and conjectured that "collision-induced V → E (vibrational to electronic) energy transfer from vibrationally excited ground state molecules" could be responsible for the $\tilde{A}\ ^2$A′ → $\tilde{X}\ ^2$A″ transition. Figure 3 depicts the three low-lying ethylperoxy radical states' ($\tilde{X}\ ^2$A″, $\tilde{A}\ ^2$A′, and $\tilde{B}\ ^2$A″) PES's relative to each other and sketches the possible interactions described above.

For ethylperoxy radical, Clifford et al.[20] (with the work of Zabel et al.[34] in mind) commented that asymmetric a″ vibrational modes could distort the structure of the activated complex and break its planar symmetry (i.e., a Herzberg—Teller type effect[35]). Through the use of spin-polarized density functional theory coupled with Born—Oppenheimer molecular dynamics (BOMD), we explore here the nuclear dynamics along the concerted-elimination path to ethylene and hydroperoxy radical and investigate how nuclear motion affects the electronic wavefunction. Though we are confined to the ground-state Born—Oppenheimer surface, our results are strongly suggestive that vibronic transitions due to symmetry-breaking of the TS1 structure (and intermediates along the reaction path of P3) are involved in the formation of ethylene and hydroperoxy radical. This vibrationally-induced symmetry breaking at the transition state provides a mechanism for neutral H-transfer, in addition to the O_2 π^*-resonance mechanism discussed above. In particular, distortions of the transition state structure render the ^{2}A′ state energetically and dynamically accessible in the neighborhood of TS1, thereby facilitating neutral hydrogen transfer. Additionally, ^{2}A′—^{2}A″ mixing is observed along all regions of the reaction path (entrance channel, ethylperoxy intermediate, and product region), suggesting this vibronic mixing is an important component of the reaction dynamics.

II. Theoretical Methods

A. Molecular Dynamics Integration. All Born—Oppenheimer molecular dynamics (BOMD) simulations in this work were generated using the *Jaguar* version 4.1 *ab initio* program[36] interfaced with a velocity-Verlet[37] dynamics code written within our research group.[38] In BOMD, the potential energy surface (PES) and the forces are calculated "on the fly" and self-consistently. The velocity-Verlet algorithm was used to integrate Newton's equations of motion.[37] Since we are using classical dynamics to propagate the nuclei, we have replaced all hydrogen atoms with deuterium atoms to minimize the error associated with neglecting quantum tunneling. CD_3CD_2 + O_2 collision trajectories and trajectories starting from the barrier (in both directions) were run for about 1 picosecond. The time step for integration was chosen to be about 0.25 fs (10 au). The drift in the total energy was, on the average, about 10^{-7} hartrees. Three collision trajectories and three pairs of TS1 barrier trajectories (forward and backward along the reaction coordinate) were performed. We acknowledge that many more trajectories would be required for a quantitative analysis of CD_3CD_2 + O_2 dynamics; our study, therefore, is to gain *qualitative* insight into this complex reaction.

B. Electronic Structure. The level of theory chosen for the generation of the PES and forces used in the dynamics simulations was spin-polarized density functional theory (DFT). The specific DFT functional chosen in this work was the B3LYP hybrid exchange-correlation functional[39] which has the Becke-3 parameter (B3) form:[40] $E_{xc} = (1 - a)E^{Slater}X + aE^{exact}X + b\Delta E^{B88}X + E^{VWN}C + c\Delta E^{LYP}C$, where "Slater" stands for the Slater exchange functional,[41] "exact" stands for the Hartree—Fock exchange, "B88" stands for the Becke 88 generalized-gradient approximation (GGA) exchange functional,[42] "VWN" stands for the Vosko—Wilk—Nusair local spin density approximation (LSDA) correlation functional,[43] "LYP" stands for the Lee—Yang—Parr gradient-corrections to the LSDA correlation functional,[44] and a, b, and c are parameters fitted to experimental atomization energies ($a = 0.2$, $b = 0.72$, and $c = 0.81$). The B3LYP functional was chosen to represent the PES in the BOMD simulations because of its comparable accuracy for thermochemistry of the CH_3CH_2 + O_2 system with that of high-quality CCSD(T) calculations (see Rienstra-Kiracofe et al.[12]) and its reasonable performance in reproducing related bond dissociation energies.[45] The basis set used in the DFT calculations was the 6-31G** basis set of Pople et al.[46—48] which consists of (4s,1p)/[2s,1p] contractions for hydrogen and (10s,4p)/[3s,2p] contractions for oxygen and carbon. The self-consistent unrestricted B3LYP-DFT energy convergence was set to 10^{-6} hartrees, all one- and two-electron integrals were evaluated analytically, and a fine grid was employed (84,330 grid points in total) for the exchange-correlation energy.

Vertical excitation energies presented in the next section were calculated using the *MOLPRO* quantum chemistry suite.[49] These

calculations were done with *MOLPRO* because it allows one to tailor an unrestricted Hartree−Fock (UHF) $^2A'$-constrained wavefunction to be used as an initial guess for a subsequent $^2A'$-constrained UDFT calculation. The *MOLPRO* package uses the VWN5 local correlation (LDA) functional of Vosko, Wilk, and Nusair[43] for its B3LYP functional rather than the original VWN[43] that *Jaguar* uses in its B3LYP functional. For vertical excitation energies, only the relative energies, rather than the absolute total energies, are important. We checked the agreement between the B3LYP functional of *MOLPRO* and that of *Jaguar* for the O_2 singlet−triplet vertical excitation energy. For this case, *MOLPRO*'s vertical excitation energy is only 0.009 eV higher than that of *Jaguar*, suggesting only a small sensitivity to which version of VWN correlation functional is employed.

C. Initial Conditions. *1. Trajectories Starting from TS1.* Initial coordinates and velocities for the simulations starting at TS1 were chosen using the quasiclassical method as formulated by Hase and co-workers.[51,50] This formulation has been implemented as a subroutine[52] into our molecular dynamics suite of codes.[38] In this method, Hessian eigenvalues and eigenvectors are required; therefore, a frequency analysis at the TS1 transition state using DFT analytic second-derivatives as implemented in *Jaguar*[36] was used to acquire this Hessian information. At the transition state, there are $3 \times 9 - 7 = 20$ degrees of freedom (one degree of freedom corresponds to the reaction coordinate and the remaining six correspond to the rotational and translational degrees of freedom omitted from these simulations). Only the zero-point vibrational energy was distributed among the normal modes. Phases were chosen from a random distribution for each of the normal modes. The normal mode displacements and velocities were then transformed to Cartesian displacements and velocities using the Hessian eigenvectors. Energy (0.3 kcal/mol) was added to the reaction coordinate to allow movement along the reaction coordinate as prescribed by Doubleday et al.[53] A spurious angular momentum arises from the harmonic normal mode approximation; this excess angular momentum was removed. Since we are dealing with classical dynamics simulations, the velocities and displacements are scaled to the desired energy. Spurious angular momentum arising from the rescaled velocities is projected out once again. The rescaling is then repeated. The repetition of rescaling followed by removal of spurious angular momentum is repeated until the kinetic energy of the scaled velocities is within about 0.1% of the desired kinetic energy. With this in mind, the desired energy (the zero-point energy) for deuterated TS1 was 31.7 kcal/mol (1.37 eV). The initial velocities chosen along the reaction path pushed TS1 toward the products $CD_2{=}CD_2 + DOO$. To run the simulation in reverse (i.e., TS1 $\rightarrow$ CD_3CD_2OO), the signs of the initial velocities were reversed.

2. Collision between Ethyl Radical and O_2. Again, the quasiclassical technique was used to initialize the coordinates and velocities of ethyl radical and molecular oxygen. In the collision of O_2 and ethyl radical, only one orientation of the O_2 position with respect to the ethyl radical was considered. The carbons of the ethyl radical, one of the methyl hydrogens, and the oxygen atoms were coplanar, and the O−O bond and the C−C bond were parallel to each other. The O_2 molecule's center-of-mass was offset from the ethyl radical's center-of-mass by a distance of about 3.5 Å. These initial coordinates were chosen to maximize the likelihood of formation of ethylperoxy radical. The coplanar transition state, TS1, is also suggestive of this collision geometry being a reasonable choice. After initialization of the velocities of each reactant molecule separately (using the same method as in initialization of the trajectories starting from TS1), CD_3CD_2 contained 28.0 kcal/mol (1.27 eV) of zero-point internal energy and O_2 contained 2.4 kcal/mol (0.10 eV) of zero-point internal energy. To give O_2 some initial translational motion, translational velocities, directed straight toward the ethyl radical, of each oxygen atom in O_2 were randomly chosen from a Maxwell−Boltzmann distribution at 300 K. After placement of ethyl radical with O_2 (3.5 Å from one another), positions and velocities were shifted to the center-of-mass frame for the $CD_3CD_2 + O_2$. We recognize that a thorough treatment of the collision between ethyl radical and O_2 should include consideration of every possible orientation and direction that O_2 could collide with ethyl, but this would entail a computationally prohibitive number of trajectories. Our purpose here is simply to probe roughly the finite temperature nuclear dynamics and evolution of the electronic wavefunction in the regions of the PES involved in concerted formation of ethylene and HOO, namely, formation of ethylperoxy radical and traversal of TS1.

D. Analysis. Since the nuclei are propagated on the ground-state Born−Oppenheimer potential energy surface, these BOMD simulations are adiabatic in nature. Therefore, use of the term "vibronic mixing," suggestive of a diabatic-state picture, may appear inconsistent given that we simulate the adiabatic dynamics. However, introduction of vibrational degrees of freedom via our choice of initial conditions allows mixing of these diabatic states, which is observed as symmetry-breaking in an adiabatic simulation. To probe this symmetry-breaking of the electronic wavefunction, we need to view changes in the shape of the highest-energy singly-occupied molecular orbital (SOMO) amplitude as time progressed in these trajectories. However, the SOMO is not always well-defined in a spin-polarized DFT calculation. We determined the identity of the SOMO by examining two highest-energy occupied α and the highest-energy occupied β-spin-orbitals along each trajectory. At each time step examined, one α-spin-orbital had high overlap with the highest lying β-spin-orbital, and these two could then be thought of as an "electron pair". The remaining α-spin-orbital was then identified as the SOMO. One other issue to bear in mind is the nature of the a″ SOMO. When either the ethylperoxy radical or the TS1 structure is constrained to C_s symmetry, the a″ SOMO is located solely on the two oxygen centers (an O_2 π^*-like orbital). When the symmetry is lowered to C_1 symmetry by torsions or antisymmetric vibrations, the a″ SOMO can mix with other orbitals. In our analysis, we determined if mixing of the a″ SOMO with other orbitals is occurring, by inspecting whether the a″ SOMO has only O_2 π^* character; any significant deviation from pure O_2 π^* character signified mixing of σ character into the a″ SOMO.

These SOMO amplitude plots were rendered using *MOLDEN*.[54] Orbital amplitude "snapshots" were rendered from one representative trajectory for the collision between CD_3CD_2 and O_2, and for one representative pair of forward and backward trajectories from TS1. Renderings were made at 100 fs intervals for the collision trajectories, and renderings for the pair of TS1 trajectories were made at 5 fs intervals.

Normal mode motion graphics were rendered using the *MOLEKEL*[55] visualization software. We also calculated the vibrational power spectrum for DOO produced in the TS1 $\rightarrow$ $CD_2{=}CD_2 + DOO$ trajectory, from the Fourier transform of the autocorrelation function of the velocities of the nascent DOO.

III. Results and Discussion

A. Energetics of the Concerted-Elimination Path. To lay the foundation for our dynamics simulations, we first discuss

TABLE 1: Thermochemistry of the Species along the Concerted-Elimination Path[a]

species	total energy	ZPVE[b]	ΔH_0 (UB3LYP)[c]	ΔH_0 (CCSD(T))[d]	corr. (298 K)[e]	ΔH_{298} (UB3LYP)	ΔH_{298} (expt.)[f]
$CH_3CH_2(^2A') + O_2(^3\Sigma_g^-)$	−229.485199	39.8	0.0	0.0	0.0	0.0	0.0
CH_3CH_2OO-*gauche*(^2A)	−229.542385	45.1	−30.6	−30.3	−0.8	−31.4	-35.5 ± 2.0[g] -35.7 ± 2.3[h]
CH_3CH_2OO-*trans*($^2A''$)	−229.541804	45.0	−30.3		−0.8	−31.1	
CH_3CH_2OO-*cis*($^2A''$)	−229.539162	44.6	−29.0		−0.8	−29.8	
TS1($^2A''$)	−229.491007	41.0	−2.4	−0.9	−0.2	−2.6	
$CH_2{=}CH_2(^1A_g) + HOO(^2A'')$	−229.497822	40.9	−6.8	−12.8	−0.5	−7.3	13.2 ± 0.5[i]
deuterated species							
$CD_3CD_2(^2A') + O_2(^3\Sigma_g^-)$	−229.485199	30.4	0.0		0.0	0.0	
CD_3CD_2OO-*gauche*(^2A)	−229.542385	34.8	−31.5		−0.7	−32.2	
CD_3CD_2OO-*trans*($^2A''$)	−229.541804	34.7	−31.2		−0.6	−31.8	
CD_3CD_2OO-*cis*($^2A''$)	−229.539162	34.4	−29.8		−0.6	−30.4	
TS1($^2A''$)	−229.491007	31.7	−2.3		−0.1	−2.2	
$CD_2{=}CD_2(^1A_g)$+DOO($^2A''$)	−229.497822	31.3	−7.0		−0.2	−6.8	

[a] Total energies are in hartrees; other values are in kcal/mol. Zero-point (ΔH_0) and thermally corrected (ΔH_{298}) enthalpies are relative to the reactant (ethyl radical and O_2) enthalpies. [b] Zero-point vibrational energy from UB3LPY/6-31G** calculations. [c] This work. All values calculated within the *Jaguar* code.[36] [d] From Rienstra-Kiracofe et al.[12] [e] Thermal correction calculated from constant-pressure heat capacities at 298 K obtained within the *Jaguar* code using the formula $\int_0^{298}[C_p(\text{products}) - C_p(\text{reactants})]\,dT$, where C_p is the heat capacity at constant pressure and T is the temperature. The correction is with respect to the reactants, ethyl radical and O_2. [f] CH_3CH_2 $\Delta_f H_{298}$ used to derive experimental $\Delta_{rxn}H_{298}$'s from Berkowitz et al.[25] [g] Knyazev and Slagle kinetics modeling of experimental data.[56] [h] Blanksby et al.[27] derived from negative-ion photodetachment spectroscopy, gas-phase acidities, and complete basis-set (CBS/APNO or CBS-Q) data; see reference for details. [i] From HOO $\Delta_f H_{298}$ of Howard[73] and $CH_2{=}CH_2$ $\Delta_f H_{298}$ of Gurvich et al.[74]

the energetics of the concerted-elimination path calculated at the UB3LYP/6-31G** level of theory and compare that to experimental observations[56,27] and the theoretical work of Schaefer and co-workers.[11,12] The enthalpies of the hydrogenated and deuterated species along the concerted-elimination path are listed in Table 1. For the exothermicity of the formation of ethylperoxy radical from ethyl radical and O_2, our results agree well with the DFT-UB3LYP calculations of Ignatyev et al.[11] (as expected) and the CCSD(T) calculations of Rienstra-Kiracofe et al.[12] but are a few kilocalories per mole less exothermic than the enthalpy of reaction at 298 K (with respect to ethyl radical and O_2) suggested by Knyazev and Slagle[56] and Blanksby et al.[27] The overall exothermicity to form HOO + $CH_2{=}CH_2$ is underestimated by about 6 kcal/mol by UB3LYP, compared to both CCSD(T) and experiment. However, the relative energy of TS1 is within 1.5 kcal/mol of that predicted by CCSD(T); it is this relative energy that is critical to reproduce, since we focus on dynamics near TS1 at this level of theory.

Structural conformations of the ethylperoxy radical have been included in Table 1 to demonstrate changes in the energetics due to internal rotations about the C−O bond. Ignatyev et al.[11] and Rienstra-Kiracofe et al.[12] found that the gauche conformation is the lowest-energy conformation of the ethylperoxy radical. The *cis* and *trans* conformations are slightly higher in energy than the *gauche* conformation, presumably due to the increased repulsions between the CH_3 group and the oxygen lone pairs in these conformations (see the Newman projections along the C−O bond[57] shown in Figure 4). According to our calculations at the UB3LYP/6-31G** level of theory, the trans conformation has a harmonic frequency of 77 cm^{-1} corresponding to the C−C−O−O torsion, in reasonable agreement with Rienstra-Kiracofe et al.'s[12] value of 94 cm^{-1} at the CCSD(T)/DZP level of theory. We find a difference in total energies between the *gauche* conformation and the *trans* conformation of 0.4 kcal/mol, which is only 0.1 kcal/mol higher than the CCSD(T)/DZP prediction of Rienstra-Kiracofe et al.[12] We find that the *cis* conformation, however, has an imaginary harmonic frequency (131*i* cm^{-1}) for the C−C−O−O torsion. This is in perfect agreement with the CCSD(T)/DZP value of 131*i* cm^{-1} calculated by Rienstra-Kiracofe et al.[12] This suggests that the

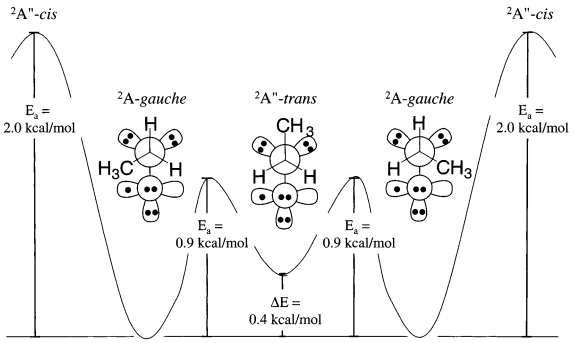

Figure 4. Newman diagrams showing the relative energies of the *gauche* and *trans* conformations of ethylperoxy radical.[57] The *gauche* and *trans* conformations are minima; E_a is the torsional barrier energy (along the C−O bond coordinate) required to access these minima. Note that the *cis* conformation of ethylperoxy radical is a torsional transition state.

cis conformation is a torsional transition state for rotation about the C−O bond. This barrier is slight (we find $\Delta E = 2.0$ kcal/mol, compared to 2.4 kcal/mol according to Rienstra-Kiracofe et al.[12]). There is an even smaller barrier going from the *gauche* to the *trans* conformations of about 0.9 kcal/mol, according to our work (1.2 kcal/mol according to Rienstra-Kiracofe et al.[12]). *As we shall see, these small barriers to internal rotations are a key feature in the dynamics of the oxidation of ethane to ethylene*.

Table 2 compares lowest-lying vertical excitations for various species at the UB3LYP/6-31G** level of theory with the CCSD(T) results of Rienstra-Kiracofe et al.[12] Our vertical excitation (T_e) energies are slightly higher than those of Rienstra-Kiracofe at al.[12] As expected, the theoretical vertical T_e's are larger than the adiabatic T_0's measured experimentally. The greatest discrepancy between our results and experiment is seen in the O_2 case, where the $^1\Delta_g - {}^3\Sigma_g^-$ splitting predicted by UB3LYP is 0.72 eV higher than experiment. This is due to the fact that the single-determinant DFT "wavefunction" cannot describe the inherently multideterminant character of the $^1\Delta_g$ state of O_2. The singlet state calculated within DFT is not pure $^1\Delta_g$ and

TABLE 2: Vertical Excitation Energies (VT_e) from the Ground-State to the Lowest-Lying Excited State for O_2, HOO, CH_3CH_2OO, and TS1[a]

species	$^3\Sigma_g^-$	$^1\Delta_g$	VT_e (UB3LYP)[b]	VT_e (CCSD(T))[c]	T_0 (expt)
O_2	−150.319976 $^2A''$	−150.257403 $^2A'$	1.70		0.9699 ± 0.0001[d]
HOO	−150.840317	−150.804610	0.97		0.8716 ± 0.0004[e] 0.872 ± 0.007[f]
CH_3CH_2OO-*trans*[i]	−229.419723	−229.382295	1.02	0.88	0.9414 ± 0.0007[g] 0.938 ± 0.004[h]
TS1	−229.369019	−229.296480	1.97	1.92	

[a] Total energies (second and third columns) are in hartrees and the vertical excitation energies are in electronvolts. [b] This work. VT_e stands for the vertical excitation energy from the bottom of the ground-state potential well. O_2 UB3LYP/6-31G** values calculated with *Jaguar*;[36] *MOLPRO*[49] was used for the other molecules. Differences in total energies between *MOLPRO* and *Jaguar* (see entries in Tables I and II) are due to the use of either VWN or VMN5 LDA correlation functionals. See text and elsewhere[43] for details. [c] From Rienstra-Kiracofe et al.[12] [d] From Huber and Herzberg; $T_e = 0.9817 \pm 0.0001$ eV.[29] [e] From Fink and Ramsey.[69] [f] From Ramond et al.[75] [g] From Hunziker and Wendt.[28] Difference in *gauche* or *trans* configurations is not noted. [h] From Blanksby et al.[27] [i] We cannot calculate excitation energies from the *gauche* conformation. Since it has no point group symmetry, only the ground state may be calculated within time-dependent DFT.

TABLE 3: Reactant, Intermediate, Transition State, and Product Harmonic Frequencies (in cm^{-1}) Calculated at the Unrestricted B3LYP-DFT/6-31G Level of Theory**

mode	CH_3CH_2 ($^2A'$)	O_2 ($^3\Sigma_g^-$)	CH_3CH_2OO (^2A-*gauche*)	TS1 ($^2A''$)	TS2 (^2A)	$CH_2{=}CH_2$ (^1A_g)	HOO ($^2A''$)
ω_1	3160(a′)	1657	3152	3179(a′)	3216	3158(a_g)	3588(a′)
ω_2	3056(a′)		3134	3123(a′)	3121	1715(a_g)	1427(a′)
ω_3	2964(a′)		3127	1626(a′)	3097	1389(a_g)	1176(a′)
ω_4	1497(a′)		3076	1586(a′)	3037	1071(a_u)	
ω_5	1482(a′)		3057	1480(a′)	1735	3218(b_{1g})	
ω_6	1414(a′)		1519	1357(a′)	1510	1243(b_{1g})	
ω_7	1072(a′)		1500	1295(a′)	1468	979(b_{1u})	
ω_8	988(a′)		1494	1039(a′)	1351	963(b_{2g})	
ω_9	494(a′)		1420	1004(a′)	1247	3244(b_{2u})	
ω_{10}	3261(a″)		1381	628(a′)	1171	834(b_{2u})	
ω_{11}	3102(a″)		1310	526(a′)	1107	3142(b_{3u})	
ω_{12}	1497(a″)		1210	366(a′)	1051	1484(b_{3u})	
ω_{13}	1200(a″)		1163	1060*i*(a′)	972		
ω_{14}	814(a″)		1210	3269(a″)	915		
ω_{15}	167(a″)		1163	3204(a″)	907		
ω_{16}			1102	1328(a″)	874		
ω_{17}			1001	1230(a″)	688		
ω_{18}			850	897(a″)	554		
ω_{19}			802	833(a″)	436		
ω_{20}			527	472(a″)	276		
ω_{21}			359	218(a″)	2212*i*		

thus is artificially destabilized, leading to an overestimated singlet−triplet gap. For the cases of HOO and CH_3CH_2OO, much better agreement with experiment is found. Our vertical T_e results are only 0.08−0.10 eV higher than the experimental T_0's for both HOO and CH_3CH_2OO. The excited states of HOO and CH_3CH_2OO do not have multiconfigurational character and hence are better described within DFT-B3LYP. We therefore conclude that as long as our simulations do not explicitly consider $^1\Delta_g$ O_2, but rather only the CH_3CH_2OO ($^2A'$) radical with which it correlates, our calculations will be reasonably accurate, from the point of view of reaction exothermicity (within 0.1−0.2 eV), relative energy of the transition state (within 0.1 eV), and placement of the $^2A'$ excited states of ROO (within 0.1 eV).

B. Comments on the Normal Modes at TS1. In addition to assessing the energetics of the $CH_3CH_2 + O_2$ reaction, some remarks about the normal modes of TS1 and deuterated TS1 are warranted. Normal modes for all the species considered are listed in Tables 3 (hydrogenated) and 4 (deuterated). Hydrogenated and deuterated TS2 normal-mode frequencies have also been included in these tables for comparison, since these two transition-state structures are similar (except for the shorter O−O bond length and the longer, extremely stretched, C−O bond in TS1) but connect to different minima. Another reason for the comparison between TS1 and TS2 is the possible curve-crossing "interplay" between paths P2 (isomerization) and P3 (concerted-elimination) conjectured by Rienstra-Kiracofe et al.,[12] Stark,[33] and Pilling and co-workers.[31,32] Soft-mode frequencies (<1000 cm^{-1}) typical of torsions are higher for TS2 than for TS1, whereas the high frequencies for C−H(−D) (>3000 cm^{-1} for hydrogenated species and >2000 cm^{-1} for deuterated species) tend to be higher for TS1 than for TS2. This is as expected since TS1 is a "looser" transition state than TS2 and, therefore it would have lower torsional normal modes; as for the higher C−H(−D) stretch modes, TS1 is more "product-like" than TS2 and, therefore, would have "stiffer" C−H(−D) bonds due to the ethylene character of the $CH_2{=}CH_2$ component of TS1. Interestingly, the imaginary frequency of the TS2 reaction coordinate is more than twice as large as that for TS1. The imaginary frequency for TS2 is consistent with a partial bond C···H stretching mode estimated by Benson[58] to be about 2200 cm^{-1}. The imaginary frequency of TS1 seems to be more consistent with a bend rather than with a stretching mode. Incidentally, Rienstra-Kiracofe et al.[12] noted that their imaginary frequency for TS1, 1389*i* cm^{-1}, is close to the 1638*i* cm^{-1} reaction coordinate frequency of "TS2" Wagner et al.[16] used in their RRKM modeling.

For deuterated TS1 considered in our BOMD simulations, there are 13 symmetric (a′) modes (including the reaction coordinate) and 8 asymmetric (a″) modes. There is a wide range

TABLE 4: Reactant, Intermediate, Transition State, and Product (deuterated) Harmonic Frequencies (in cm^{-1}) Calculated at the Unrestricted B3LYP-DFT/6-31G Level of Theory**

mode	CD_3CD_2 ($^2A'$)	O_2 ($^3\Sigma_g^-$)	CD_3CD_2OO (^2A-*gauche*)	TS1 ($^2A''$)	TS2 (^2A)	$CD_2{=}CD_2$ (^1A_g)	DOO ($^2A''$)
ω_1	2299(a′)	1657	2339	2325(a′)	2394	2341(a_g)	2615(a′)
ω_2	2244(a′)		2328	2266(a′)	2303	1594(a_g)	1194(a′)
ω_3	2144(a′)		2320	1440(a′)	2263	1013(a_g)	1042(a′)
ω_4	1213(a′)		2236	1366(a′)	2207	796(a_u)	
ω_5	1075(a′)		2197	1147(a′)	1248	2399(b_{1g})	
ω_6	1065(a′)		1219	1096(a′)	1169	1008(b_{1g})	
ω_7	901(a′)		1186	997(a′)	1114	758(b_{1u})	
ω_8	778(a′)		1108	829(a′)	1078	740(b_{2g})	
ω_9	376(a′)		1084	774(a′)	985	2415(b_{2u})	
ω_{10}	2431(a″)		1081	595(a′)	960	600(b_{2u})	
ω_{11}	2291(a″)		1077	473(a′)	939	2270(b_{3u})	
ω_{12}	1086(a″)		1008	340(a′)	898	1099(b_{3u})	
ω_{13}	968(a″)		962	825*i*(a′)	847		
ω_{14}	587(a″)		921	2437(a″)	793		
ω_{15}	118(a″)		843	2386(a″)	759		
ω_{16}			736	1003(a″)	691		
ω_{17}			600	923(a″)	572		
ω_{18}			468	645(a″)	489		
ω_{19}			321	599(a″)	350		
ω_{20}			175	343(a″)	227		
ω_{21}			105	200(a″)	1632*i*		

of a″ vibrational modes: 200, 343, 599, 645, 923, 1003, 2386, and 2437 cm^{-1}, all of which can contribute to Herzberg−Teller type interactions[35] at the saddle point; that is, rapid perturbations to the C_s symmetry of TS1, to first order, caused by antisymmetric a″ modes (especially low-energy torsional modes) can reduce the symmetry of TS1 from C_s symmetry to C_1 symmetry, so that the $^2A''$ and $^2A'$ diabatic states can interact, thereby facilitating neutral H-transfer (as in Figure 2a). Since the vertical excitation energies of both ethylperoxy radical and hydroperoxy radical are less than 1 eV (see Table 2), invocation of the Herzberg-Teller effect is reasonable, since Herzberg has noted that the first-order term become significant when the states in question are roughly less than 1 eV.[59] Statistically, the soft-mode vibrational states are more likely to be populated than those for the higher stretching frequencies. The soft modes (200−1003 cm^{-1}) are basically asymmetric torsions and symmetric ring-distortions. The mid-frequency modes (1096−1440 cm^{-1}) are ring-distortions involving a significant amount of O−O or C−C stretching and D−C−D symmetric bending. The higher frequency modes (2266−2437 cm^{-1}) are asymmetric and symmetric, ethylene-like D−C−D stretching modes. Figure 5 shows selected normal modes at TS1 representing six general types of motion: low-frequency asymmetric torsion (a″, 645 cm^{-1}), low-frequency symmetric ring-distortion (a′, 774 cm^{-1}), mid-frequency symmetric ring-distortion (a′, 1147 cm^{-1}; this particular mode involves significant O−O stretching), high-frequency C−D symmetric stretching (a′, 2325 cm^{-1}), high-frequency asymmetric stretching (a″, 2386 cm^{-1}), and the symmetric reaction coordinate motion (a′, 825*i* cm^{-1}). It is the low-frequency asymmetric torsion of a″ symmetry to which we will return in our analysis below.

C. $CD_3CD_2 + O_2 \rightarrow CD_3CD_2OO^*$ Dynamics. Because of the large exothermicity (∼35 kcal/mol) of the $CD_3CD_2 + O_2 \rightarrow CD_3CD_2OO$ reaction and the fact that *ab initio* calculations[11,12] have shown that this reaction is barrierless, it is not surprising that we see facile addition of O_2 to ethyl radical to form the ethylperoxy complex. The attraction between the radical center on the ethyl radical and an unpaired electron on O_2 is strong and appears to be long-ranged. The origin of this long-ranged attraction has been studied in detail by Bayes and co-workers.[60−62] They showed that there is a strong correlation between alkyl radical ionization energies and the kinetic rate constants for $R\cdot + O_2$ addition. As a straight-chain alkyl radical increases in length, the ionization energy generally decreases and the corresponding rate constant for addition increases. A decrease in the ionization energy implies that the electrons of

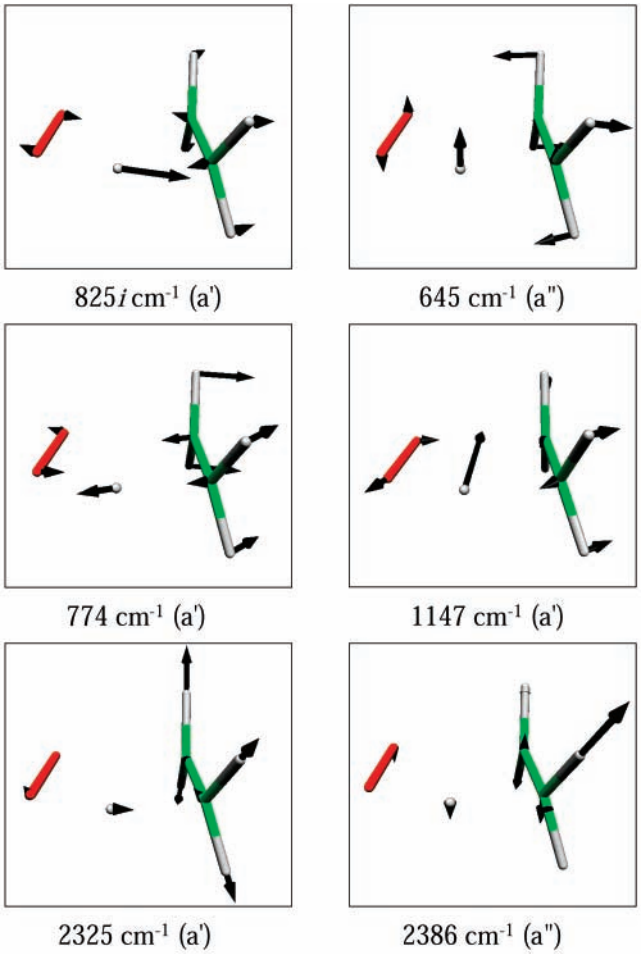

Figure 5. Selected vibrational normal modes at TS1 (deuterated). See text for the explanation of the selection from the 21 possible normal modes of TS1. O_2 is the red fragment. The green region represents the C−C component of the ethylene-like fragment. The white regions represent the hydrogen (deuterium) atoms.

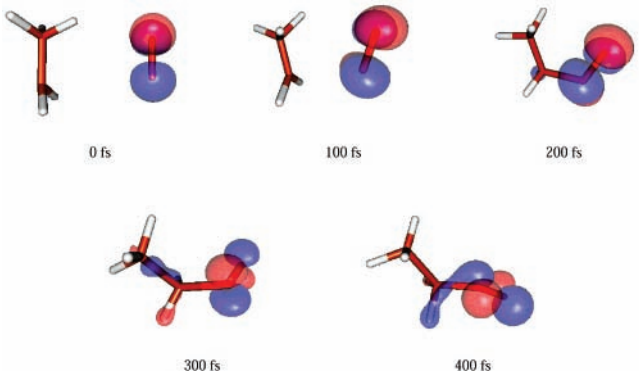

Figure 6. SOMO "snapshots" of the $CD_3CD_2 + O_2$ collision at 0, 100, 200, 300, and 400 fs. Symmetry-mixing of a″ SOMO with ethyl σ-radical orbitals is present at 300 and 400 fs. The red and blue features represent opposite orbital phases.

the radical R· are less tightly bound and easily polarizable; this increases the dipole interactions between R· and O_2 and, therefore, increases the collision cross section.[32] The "barrierless" R· + O_2 transition state is a very loose transition state (having a large collision cross section) which cannot be modeled effectively using conventional transition state theory. In the recent works of Klippenstein and co-workers,[18,19] variational transition state theory (VTST) has been successfully applied to the $CH_3CH_2 + O_2$ addition reaction in their master equation studies of ethane oxidation.

With the work of Bayes and co-workers in mind, we know that the addition of O_2 to the ethyl radical will be very attractive. We may explore the reaction cross section of this collision in future work, but in this preliminary study, we are only analyzing the orbital amplitudes along one arbitrary direct path leading to production of the vibrationally excited ethylperoxy radical. 3-D plots of the a″ highest singly-occupied molecular orbital (SOMO) appear in Figure 6 at 0, 100, 200, 300, and 400 fs. The dipole moment of this system (calculated at the B3LYP-DFT/6-31G** level) of theory increases as O_2 approaches ethyl radical, as expected from the analyses by Bayes and co-workers. The corresponding dipole moments for 0, 100, 200, 300, and 400 fs are 0.30, 1.84, 2.68, 2.62, and 3.24 D, respectively. At the beginning of the trajectory, both oxygens have the same amount of nuclear kinetic energy. Around 50 fs into the simulation, the oxygen closest to the ethyl radical center apparently "feels" a very attractive potential at about 3 Å and accelerates toward the ethyl's radical carbon center.[63] This oxygen collides with the radical carbon center around 150 fs into the simulation. Up until this time, no symmetry-breaking of the a″ SOMO is observed (times 0 and 100 fs in Figure 6). After O_2 has bonded with CD_3CD_2 at the radical carbon center, mixing of the a″ orbital with σ-like (a′) orbitals in the ethyl radical fragment is observed. This is evident by the appearance of orbital amplitude over the ethyl substituent of the newly formed ethylperoxy radical (see times 200, 300, and 400 fs in Figure 6). These results show that interaction between the ^{2}A″ ground state and lowest-lying ^{2}A′ state is possible even in the collision between ethyl radical and O_2, due to torsional motion around the newly-formed C−O bond as the ethylperoxy radical moves to adopt the more sterically favored staggered (*gauche*) conformation (see time 400 fs in Figure 6). Because of our choice of initial orientation, the ethyl radical and O_2 first form a *cis* ethylperoxy conformer, which, as discussed in Section IIIA, is a torsional transition state. Thus the newly-formed ethylperoxy complex will move toward either the *gauche* or *trans* minima. If we had chosen initial orientations favoring direct formation

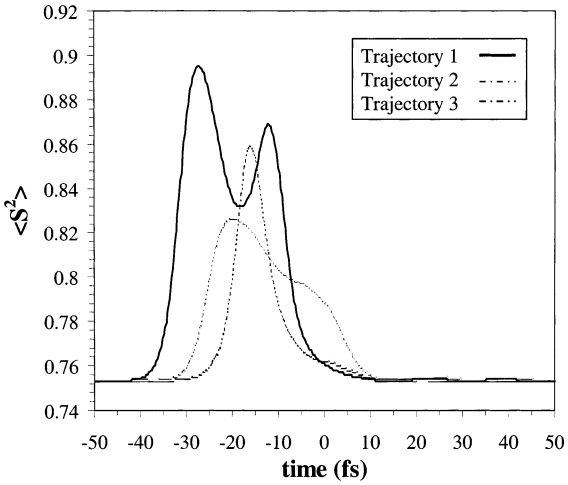

Figure 7. Profile of $<\hat{S}^2>$ for the forward and backward trajectories starting from TS1.

of the *gauche* global minimum, which has no symmetry, or the *trans* local minimum, mixing of the ^{2}A′ and ^{2}A″ states would also occur due to the very small torsional barriers between these states (see Figure 4).

D. TS1 → CD_3CD_2OO* Dynamics. The purpose of these trajectories was to determine (in reverse) the favorable peroxy radical pathways leading to TS1 and onward to dissociation, forming hydroperoxy radical and ethylene. The "fall" into the ethylperoxy radical minimum from TS1 is highly exothermic, just as it was in the case of the ethyl and molecular oxygen collision (recall Figure 1). The fall is immediate; that is, the "re-formation" of ethylperoxy takes less than 50 fs from TS1, resulting in a very vibrationally excited CD_3CD_2OO radical. A profile of $<\hat{S}^2>$ in Figure 7 shows that there is significant spin-contamination in the −50 to 0 fs time window "before" TS1. Though it is well-known that spin-contamination in spin-polarized DFT is usually small compared with that in other unrestricted single-reference methods such as unrestricted Hartree−Fock theory (UHF) and unrestricted second-order Møller−Plesset theory (UMP2),[64] the spin-contamination is quite high in this case and indicates that DFT has difficulty representing the tri-radicaloid character (exhibiting a bit of spurious quartet character) of the intermediate nuclear configurations in the trajectory between −50 and 0 fs. Renderings of the excess spin density (see Figure 8) at 5 fs intervals reveal that a high concentration of excess β-spin density is located on the ethyl group, while a high concentration of excess α-spin density is seen in the π* area along the O−O bond en route to TS1. This could be viewed as due to the incipient formation of the C−C π bond in ethylene, which leads to some nascent quartet character. Two peaks are present in the $<\hat{S}^2>$ profile (Figure 7) of the first trajectory: one at about −12.5 fs and one around −30 fs which correspond nicely to the onset of excess β-spin density on the C. Furthermore, we observe a correlation between the O−O bond length and the spin contamination seen in these trajectories; the increased triplet character of the O_2 fragment as the O−O shortens to ∼1.2 Å (about the length of isolated molecular oxygen) during the transition from CD_3CD_2OO to ethylene and DOO may be the cause. From the first trajectory, one sees that the bond shortens to about ∼1.2 Å twice during this 50 fs window: once around −9 fs and once around −35 fs. The second trajectory has a small $<\hat{S}^2>$ peak at about 5 fs and a larger peak at −22 fs: the O−O bond length in this case shortens to about 1.22 Å at both 0 fs and −24 fs, close to these peaks. The third trajectory appears to have only one peak around

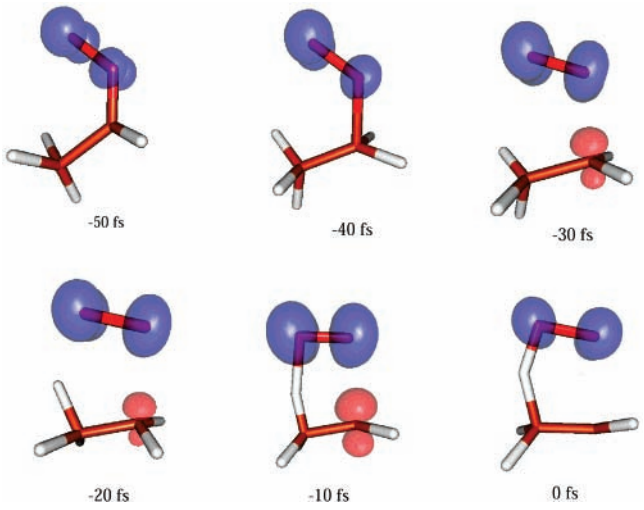

Figure 8. Snapshots of the excess spin density at 10 fs intervals −50 fs to 0 fs "before" TS1 (from Trajectory 1). The pink lobe represents the excess β density, and the blue lobes represent the excess α density.

−17 fs, and the O−O bond shortens to about 1.22 Å only once during this simulation, around −16 fs. The increased isolated molecular oxygen character provides support for the mechanism presented in Figure 2c, where the O_2 π^* resonance plays an important role in the $^2A''$ transition state to facilitate neutral H-transfer. Also relevant here is the fact that the O−O stretching mode is an active mode in the $\tilde{A}\,^2A' \leftarrow \tilde{X}\,^2A''$ transition.[27,65] Through negative-ion photodetachment spectroscopy, *ab initio* calculations, and generalized valence bond (GVB) arguments, Blanksby et al.[27] found that both the O−O stretch and the C−O−O bends in CH_3OO and CH_3CH_2OO are active modes in the $\tilde{A} \leftarrow \tilde{X}$ transition. Pushkarsky et al.[65] also observed O−O stretching in this transition in their cavity ring-down spectroscopy experiments on the CH_3OO radical. From GVB diagrams alone, exciting the O−O stretch is expected because of the repulsion between the oxygen lone-pairs in the $^2A'$ state of ROO. Elongated O−O bonds in the $^2A'$ ROO species are depicted in Figures 2d and 3 to illustrate this point.

In viewing the SOMO at 10 fs interval in these trajectories, mixing of the pure a″ π^*-like SOMO localized on the oxygen atoms with the a′ σ-orbitals of ethyl radical is evident, just as it was in the case of the collision between CD_3CD_2 and O_2. In Figure 9, the orbitals labeled with times from −50 to 0 fs represent the $CD_3CD_2OO \rightarrow$ TS1 orbital amplitude plots. Mixing of the a″ SOMO with σ-orbitals of the ethyl group of the ethylperoxy radical is evident in the −50 and −40 fs orbital amplitude plots, where the C−O bond is still intact. At times leading up to TS1 (−30, −20, −10, and 0 fs), mixing of the a″ orbital was not observed. Significant spin contamination was observed only in these times within the −35 to 0 fs interval; for the times showing significant mixing (−50 and −40 fs "before" TS1), spin contamination is minimal (see Figure 7), indicating that the $^2A'-^2A''$ mixing is not an artifact of spin-contamination of the DFT wavefunction. These results show that $^2A''-^2A'$ interaction is also possible on the opposite side of the ethylperoxy potential well. When ethylperoxy radical is formed from either side of the ethylperoxy potential well, the ethylperoxy complex gains 29−30 kcal/mol of vibrational energy; this amount of energy is more than 1 eV (the energy needed for the $\tilde{A}\,^2A' \leftarrow \tilde{X}\,^2A''$ excitation of ethylperoxy radical), and therefore the $^2A'$ state is energetically accessible. Moreover, the low barriers to torsional motion make the $^2A'$ state available dynamically.

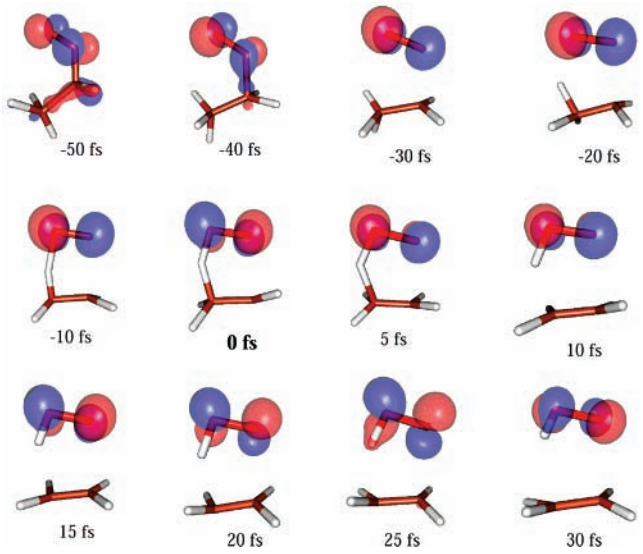

Figure 9. Snapshots of the a″ SOMO at 10 fs intervals from −50 fs to 0 fs (referenced from TS1) and at 5 fs interval from 0 to 30 fs following TS1. Symmetry-mixing of a″ SOMO is seen at −50, −40, and +25 fs. The red and blue features represent opposite orbital phases.

E. TS1 → CD_2═CD_2 + DOO Dynamics. Examination of these trajectories reveals that the DOO radical and CD_2═CD_2 do not break from each other in a symmetric fashion (i.e., with all carbons, oxygens, and the in-plane hydrogen coplanar and the other hydrogens symmetrically above and below the mirror plane). The deuterium of DOO slowly swings above and below the plane of symmetry after DOO breaks away from ethylene. The ethylene fragment also slowly rocks back and forth upon breaking away from the DOO radical. The D−O bond stretching is very vibrationally energetic. Also, the O−O fragment appears to rotate in one direction perpendicular to the C_s mirror plane, and the C−C rotates counter to the O−O fragment's rotation from the TS1 structure.[63] The counter-rotation is likely due to the preservation of $J = 0$ (as angular momentum was removed in the selection of the initial conditions).

As in the previous sections, we see symmetry mixing of the SOMO. Plots of the orbital amplitude from 0 to 30 fs at 5 fs intervals of the a″ SOMO appear (following the plots for CD_3-$CD_2OO \rightarrow$ TS1 from −50 to 0 fs) in Figure 9 for TS1 → CD_2═CD_2 + DOO. At about 25 fs into the trajectory, mixing of the a″ SOMO with the a′ π^*-like orbital occurs. The amplitude plot of the a″ SOMO at the preceding time (20 fs) is tilted at an angle with respect to the plane of symmetry of TS1. Spin contamination is negligible after TS1 (see Figure 7, Trajectory 1, after time = 0 fs). Therefore, again the symmetry-breaking here is not due to some spurious effect of spin-contamination. The a″ SOMO is exclusively on the DOO radical in this set of trajectories. Isolated HOO (and DOO) itself has interesting properties, which we now discuss.

From the spectra of Tuckett et al.,[66] the structures of the $^2A''$ ground state and the lowest-lying $^2A'$ excited state of HOO have been determined to be only slightly different. The O−H bond lengths for $\tilde{X}\,^2A''$ and $\tilde{A}^2A'$ are 0.98 and 0.97 Å, respectively. The O−O bond lengths for $\tilde{X}\,^2A''$ and $\tilde{A}\,^2A'$ are 1.33 and 1.39 Å, respectively. The H−O−O angles for $\tilde{X}\,^2A''$ and $\tilde{A}\,^2A'$ are 104.0° and 102.7°, respectively. The vertical transition, $\tilde{A}\,^2A' \leftarrow \tilde{X}\,^2A''$ is (to three decimal places) 0.872 eV.[67,68] More interestingly, Renner−Teller (the analogue of the Jahn−Teller effect for linear molecules) and spin−orbit-coupling-induced electric dipole transitions have been attributed to many of the forbidden $\tilde{A}\,^2A' \leftarrow \tilde{X}\,^2A''$ transitions reported in the spectroscopy

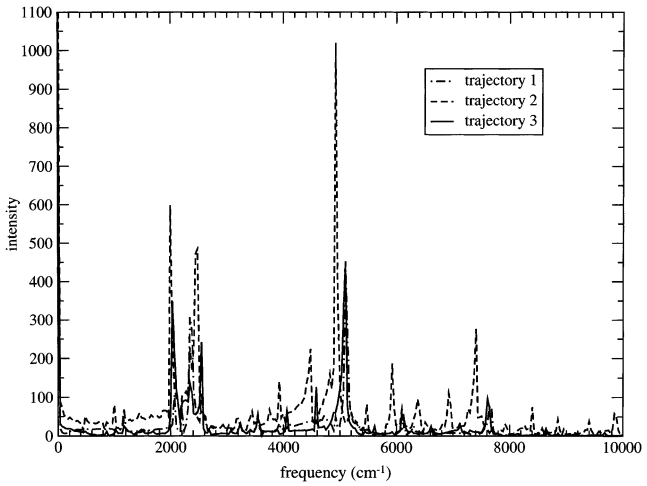

Figure 10. Fourier transform of the velocity autocorrelation function of the vibrational degrees of freedom for DOO for three trajectories, TS1 $\rightarrow D_2C{=}CD_2 + DOO$. Note that there are many more lines than the three fundamental frequencies (D−O−O bend, $\omega_{harmonic} = 1042$ cm^{-1}; O−O stretch, $\omega_{harmonic} = 1194$ cm^{-1}; and O−D stretch, $\omega_{harmonic} = 2615$ cm^{-1}). There are many small peaks occurring at intervals of 440−550 cm^{-1} starting around 3000 cm^{-1} due to coupling between all three of the DOO modes.

studies of Tuckett et al.[68,66] and Fink and Ramsay[69] and reproduced in the theoretical spectra of Ossman et al.[70] At linearity, the $\tilde{X}\,^2A''$ and $\tilde{A}\,^2A'$ states of HOO (and DOO) become degenerate, correlating with an ionic $(H^+(O_2)^-)$ $^2\Pi$ electronic state 2.7 eV above the ground state.[71] Thus, excitation of the bending mode in HOO is expected to enhance interaction between the $\tilde{X}\,^2A''$ and $\tilde{A}\,^2A'$ electronic states, which can lead to the Renner−Teller effect.

To explore the dynamics of the nuclei of DOO in our simulations, we show the Fourier Transform of the velocity autocorrelation function of the internal degrees of freedom of DOO for the three TS1 $\rightarrow CD_2{=}CD_2 + DOO$ trajectories (Figure 10). When DOO is formed from TS1, the D−O bond stretching is highly excited. In Figure 10, we see that the coupling between the three normal modes of DOO is fairly strong. We see a very small peak at around 1000 cm^{-1}, which would coincide with the D−O−O bending and O−O stretch mode fundamentals. However, we see large groups of peaks centered at ∼2200 and ∼5000 cm^{-1}. The D−O stretch is buried in the group of peaks at 2200 cm^{-1}. Coupling of the three DOO modes is evident by the extra peaks occurring about every 400−550 cm^{-1} starting around 3100 cm^{-1}. Interestingly, the difference between the O−D stretch (2615 cm^{-1}; see Table 4 for the frequencies of DOO) and twice either the O−O−D bending mode (1042 cm^{-1}) or the O−O stretching mode (1194 cm^{-1}) suggests Fermi resonances between the D−O stretch first overtone and the D−O−O bend and O−O stretch third overtones in the 5000 cm^{-1} region. In these molecular dynamics simulations, we see that the D−O stretching is very vigorous, with bond lengths oscillating between 0.87 and 1.15 Å. The D−O−O angle oscillates between, roughly, 85° and 120°. With the increase in the D−O−O bond angle, the likelihood of $\tilde{X}\,^2A''$−$\tilde{A}\,^2A'$ mixing occurring increases, because of the narrowing vertical gap between these two states as DOO approaches linearity. In-plane normal modes frequencies 595, 774, 829, 997, 1096, 1147, 1366, and 1440 cm^{-1} (see Table 4) can stimulate the D−O−O bending mode in TS1. Thus, in-plane a′ modes also may lead to Renner−Teller interactions in DOO.

Lastly, we also observe an overall in-plane rotation of the DOO fragment as it breaks away from the ethylene fragment. This was expected, since both Ignatyev et al.[11] and Rienstra-Kiracofe et al.[12] have reported a $CH_2{=}CH_2{\cdots}HOO$ van der Waals complex, with the hydrogen atom of HOO strongly attracted to the π density of the newly-formed ethylene molecule; while the hydrogen of HOO (or the deuterium in this case) is held by its electrophilic attraction for the ethylene's π-electrons, the terminal oxygen continues to leave the newly-formed ethylene fragment, thereby causing a net torque.

IV. Summary and Conclusions

In this work, we attempted to shed more light on the still elusive (and incomplete) mechanism for ethylene production in ethane oxidation by applying BOMD using forces derived from spin-polarized B3LYP-DFT. Our initial conditions consisted of small displacements from equilibrium structures and velocities along the normal coordinates, choosing the phases of these displacements randomly. Previous static quantum chemistry analyses suggested that the lowest-energy transition state may involve a counter-intuitive proton transfer (see Figure 2b). We showed via our MD simulations how this proton transfer may be avoided at finite temperature via vibrationally-induced symmetry-breaking all along the reaction path. In particular, we explored the PES along the lowest-energy P3 path in ethane oxidation from ethyl radical and molecular oxygen to ethylene and hydroperoxy radical (see Figure 1). We probed the PES in three scenarios: from the collision of CD_3CD_2 and O_2 to form vibrationally hot CD_3CD_2OO, from TS1 in the backward direction to "re-form" CD_3CD_2OO, and in the forward direction to form $CD_2{=}CD_2$ and vibrationally excited DOO. Using orbital amplitude "snapshots" at selected trajectory times, we demonstrated that mixing of the a″ SOMO occurs in all three trajectory scenarios, suggesting that $^2A''$ and $^2A'$ state mixing occurs all along the reaction path (see Figure 3). Mixing of the a″ SOMO is most evident at 300 and 400 fs into the collision of ethyl radical and O_2 (see Figure 6), −50 and −40 fs before TS1 (see Figure 9), and 25 fs following TS1 (see Figure 9). The mechanism responsible for this is torsional motion along the C−O bond in the ethylperoxy radical intermediate. Since the *cis* conformation of ethylperoxy radical is energetically unfavorable (as it is a torsional transition state), the low barrier (<2 kcal/mol) to torsional motion along the C−O bond coordinate to form the more energetically favorable *gauche* and (to a lesser extent) *trans* conformations will provide a driving force for symmetry-breaking. This symmetry-breaking allows the $^2A''$ and $^2A'$ states to mix and allows access to a state where neutral H-transfer readily occurs. Moreover, a″-symmetry vibrations at TS1 itself (a manifestation of ethylperoxy's torsional motion), along with a′-symmetry vibrations local to DOO plus the in-plane rotations of the DOO product, also act to lower the C_s symmetry of TS1. This will occur at (and increase with) finite temperature, thereby allowing neutral H-transfer to occur via the $^2A''$−$^2A'$ state mixing. The a″−a′ mixing on the DOO fragment, which we observe most evident 25 fs following the TS1 (0 fs) presented in Figure 9, is consistent with the "unavoided crossing" point along the C−O bond (most likely following the TS1 structure) suggested by Stark.[33] On the other hand, both the structure of the transition state and the high spin-contamination (due to nascent quartet spin character) correlated with the shortening of the O−O bond seen along the $CD_3CD_2OO \rightarrow$ TS1 path suggests the O_2 π^*-resonance mechanism[26] presented in Figure 2c also provides the means to avoid proton transfer. A decoupled O_2 has three electrons in each π-plane, where the π^* electrons resonate between both oxygen atoms. TS1 is a "late," product-like transition state with a short

O−O bond length and a very long C−O bond length, which allows the O_2 to decouple from the ethyl group in TS1. This π*-resonance facilitates neutral hydrogen-transfer in TS1 by allowing the in-plane unpaired π* electron to vacillate between the two oxygen centers (as shown in Figure 2c). Overall, the dynamics presented here indicate that this π*-resonance picture together with the $^2A'-^2A''$ mixing provides a more physically realistic view of the oxidative dehydrogenation mechanism than has been presented previously.

Lastly, we note that the O_2 $^1\Delta_g - {}^3\Sigma_g^-$ gap at the level of theory used here (spin-polarized B3LYP-DFT) is 1.70 eV (1.60 eV at the restricted-open B3LYP-DFT level of theory); by use of a larger 6-311G** basis set,[72] there is only a 0.01 eV decrease. These calculated splittings are much higher than experiment ($T_e = 0.9817 \pm 0.0001$),[29] due to DFT's inability to describe the multiconfiguration character of $^1\Delta_g$ O_2. On the other hand, our UB3LYP/6-31G** $^2A'-^2A''$ splittings for HOO (0.97 eV) and CH_3CH_2OO (1.02 eV for trans) are only slightly higher than experimental results (0.8716 and 0.9415 eV, respectively; see Table 2), due to the predominantly single-configuration character of these states. If we had *underestimated* this singlet−triplet gap of O_2 and the $^2A'-^2A''$ gap of HOO and CH_3CH_2OO, one might rightfully worry that the $^2A'-^2A''$ mixing we observe is simply an artifact of DFT-B3LYP, given that the $^2A'$ ethylperoxy radical correlates to $^1\Delta_g$ O_2. However, since instead DFT-B3LYP *destabilizes* $^1\Delta_g$ O_2 relative to experiment, we are biased against this $^2A'-^2A''$ mixing, yet it occurs anyway. This lends further credence to the vibronic mixing mechanism put forth here.

Acknowledgment. A.A. and E.A.C. thank Profs. G. B. Ellison and R. D. Levine and Drs. D. J. Mann, E. W. Kaiser, and W. F. Schneider for their helpful discussions. Crucial insightful comments regarding the O_2 π*-resonance mechanism by a referee are also gratefully acknowledged. Funding for this research was provided by the Ford Motor Company.

Supporting Information Available: Movies of these trajectories can be viewed at http:/www.chem.ucla.edu/dept/Faculty/carter/movies.

References and Notes

(1) Lightfoot, P. D.; Cox, R. A.; Crowley, J. N.; Destriau, M.; Hayman, G. D.; Jenkin, M. E.; Moortgat, G. K.; Zabel, F. *Atmos. Environ.* **1992**, *26A*, 1805−1961.

(2) Finlayson-Pitts, B. J.; Pitts, J. N., Jr. *Science* **1997**, *276*, 1045.

(3) Brasseur, G. P., Orlando, J. J., Tyndall, G. S., Eds.; *Atmospheric Chemistry and Global Change*; Oxford University Press: New York, 1999.

(4) Tyndall, G. S.; Cox, R. A.; Granier, C.; Lesclaux, R.; Moorgat, G. K.; Pilling, M. J.; Ravishankara, A. R.; Wallington, T. J. *J. Geophys. Res.* **2001**, *106*, 12157.

(5) Westbrook, C. K. *Chem. Ind.* **1992**, *100*, 562.

(6) Bras, G. L., Ed. *Chemical Processes in Atmospheric Oxidation: Laboratory Studies of Chemistry Related to Tropospheric Ozone*; Springer: Berlin, 1997; Vol. 3.

(7) Pilling, M. J., Ed.; *Comprehensive Chemical Kinetics: Low-Temperature Combustion and Autoignition*; Elsevier: Amsterdam, 1997; Vol. 35.

(8) Semenov, N. *Chemical Kinetics and Chain Reactions*; Oxford: London, 1935.

(9) Quelch, G. E.; Gallo, M. M.; Schaefer, H. F., III. *J. Am. Chem. Soc.* **1992**, *114*, 8239.

(10) Quelch, G. E.; Gallo, M. M.; Shen, M.; Xie, Y.; Schaefer, H. F., III; Moncrieff, D. *J. Am. Chem. Soc.* **1994**, *116*, 4953.

(11) Ignatyev, I. S.; Xie, Y.; Allen, W. D.; Schaefer, H. F., III. *J. Chem. Phys.* **1997**, *107*, 141.

(12) Rienstra-Kiracofe, J. C.; Allen, W. D.; Schaefer, H. F., III. *J. Phys. Chem. A* **2000**, *104*, 9823.

(13) Knox, J. H.; Norrish, R. G. W. *Trans. Faraday Soc.* **1954**, *50*, 928.

(14) Kaiser, E. W.; Wallington, T. J.; Andino, J. M. *Chem. Phys. Lett.* **1990**, *168*, 309.

(15) Kaiser, E. W.; Lorkovic, I. M.; Wallington, T. J. *J. Phys. Chem.* **1990**, *94*, 3352.

(16) Wagner, A. F.; Slagle, I. R.; Sarzynski, D.; Gutman, D. *J. Phys. Chem.* **1990**, *94*, 1853.

(17) Kaiser, E. W. *J. Phys. Chem.* **1995**, *99*, 707.

(18) Miller, J. A.; Klippenstein, S. J.; Robertson, S. H. In *Proceedings of the Combustion Institute 2000*, 2000; Vol. 28.

(19) Miller, J. A.; Klippenstein, S. J. *Intl. J. of Chem. Kinetics* **2001**, *33*, 654.

(20) Clifford, E. P.; Wenthold, P. G.; Gareyev, R.; Lineberger, W. C.; DePuy, C. H.; Bierbaum, V. M.; Ellison, G. B. *J. Chem. Phys.* **1998**, *109*, 10293.

(21) Benson, S. W.; Nangia, P. S. *Acc. Chem. Res.* **1979**, *12*, 223.

(22) Baldwin, R. R.; Dean, C. E.; Walker, R. W. *J. Chem. Soc., Faraday Trans. 2* **1986**, *82*, 1445.

(23) Walker, R. W.; Morley, C. Basic Chemistry of Combusion. In *Comprehensive Chemical Kinetics: Low-Temperature Combustion and Autoignition*; Pilling, M. J., Ed.; Elsevier: Amsterdam, 1997; Vol. 35.

(24) Baldwin, R. R.; Stout, D. R.; Walker, R. W. *J. Chem. Soc., Faraday Trans.* **1991**, *87*, 2147.

(25) Berkowitz, J.; Ellison, G. B.; Gutman, D. *J. Phys. Chem.* **1994**, *98*, 2744.

(26) Harding, L. B., through private communications with Ellison, G. B.

(27) Blanksby, S. J.; Ramond, T. M.; Davico, G. E.; Nimlos, M. R.; Kato, S.; Bierbaum, V. M.; Lineberger, W. C.; Ellison, G. B.; Okumura, M. *J. Am. Chem. Soc.* **2001**, *123*, 9585.

(28) Hunziker, H. E.; Wendt, H. R. **1976**, *64*, 3488.

(29) Huber, K. P.; Herzberg, G. *Constants of Diatomic Molecules*; Van Nostrand: New York, 1979.

(30) Walch, S. P. *Chem. Phys. Lett.* **1993**, *215*, 81.

(31) Pilling, M. J.; Robertson, S. H.; Seakins, P. W. *J. Chem. Soc., Faraday Trans.* **1995**, *91*, 4179.

(32) Robertson, S. H.; Seakins, P. W.; Pilling, M. J. Elementary Reactions. In *Comprehensive Chemical Kinetics: Low-Temperature Combustion and Autoignition*; Pilling, M. J., Ed.; Elsevier: Amsterdam, 1997; Vol. 35.

(33) Stark, M. S. *J. Am. Chem. Soc.* **2000**, *122*, 4162.

(34) Holstein, K. J.; Fink, E. H.; Wildt, J.; Winter, R.; Zabel, F. *J. Phys. Chem.* **1983**, *87*, 3943.

(35) Herzberg, G.; Teller, E. *Z. Physik. Chem.* **1933**, *B21*, 410.

(36) *Jaguar*, ver. 4.1, Schrödinger, Inc.: Portland, OR, 2000.

(37) Swope, W. C.; Andersen, H. C. *J. Chem. Phys.* **1982**, *76*, 637.

(38) da Silva, A. J. R.; Carter, E. A. Unpublished work.

(39) Frisch, M. J.; Trucks, G. W.; Head-Gorden, M.; Gill, P. M. W.; Wong, M. W.; Foresman, J. B.; Johnson, B. G.; Schlegel, H. B.; Robb, M. A.; Replogle, E. S.; Gomperts, R.; Andres, J. L.; Rahavachari, K.; Binkley, J. S.; Gonzalez, C.; Martin, R. L.; Fox, D. J.; Defrees, D. J.; Baker, J.; Stewart, J. J. P.; Pople, J. A. *Gaussian 92*; Gaussian, Inc.: Pittsburgh, PA, 1992.

(40) Becke, A. D. *J. Chem. Phys.* **1993**, *98*, 5648.

(41) Slater, J. C. *Quantum Theory of Molecules and Solids: The Self-Consistent Field for Molecules and Solids*; McGraw-Hill: New York, 1974; Vol. 4.

(42) Becke, A. D. *Phys. Rev. A* **1988**, *38*, 3098.

(43) Vosko, S. H.; Wilk, L.; Nusair, M. *Can. J. Phys.* **1980**, *58*, 1200. The VWN local correlation functional is presented on p 1207, and the VWN5 local correlational functional is presented on p 1209.

(44) Lee, C.; Yang, W.; Parr, R. G. *Phys. Rev. B* **1988**, *38*, 785.

(45) Andersen, A.; Carter, E. A., to be submitted for publication.

(46) Hehre, W. J.; Ditchfield, R.; Pople, J. A. *J. Chem. Phys.* **1972**, *56*, 2257.

(47) Hariharan, P.; Pople, J. *Theor. Chim. Acta* **1973**, *28*, 213.

(48) Francl, M.; Petro, W.; Hehre, W. J.; Binkley, J.; Gordon, M.; Defrees, D.; Pople, J. *J. Chem. Phys.* **1982**, *77*, 3654.

(49) Werner, H.-J.; Knowles, P. J.; Amos, R. D.; Bernhardsson, A.; Berning, A.; Celani, P.; Cooper, D. L.; Deegan, M. J. O.; Dobbyn, A. J.; Eckert, F.; Hampel, C.; Hetzer, G.; Korona, T.; Lindh, R.; Lloyd, A. W.; McNicholas, S. J.; Manby, F. R.; Meyer, W.; Mura, M. E.; Nicklass, A.; Palmieri, P.; Pitzer, R.; Rauhut, G.; Schütz, M.; Stoll, H.; Stone, A. J.; Tarroni, R.; Thorsteinsson, T. *MOLPRO*: a package of *ab initio* programs, University of Birmingham, Edgbaston, Birmingham, UK, 1999.

(50) Peslherbe, G. H.; Wang, H.; Hase, W. L. Advances in Chemical Physics: Monte Carlo Sampling for Classical Trajectory Simulations. In *Monte Carlo Methods in Chemical Physics*; Ferfuson, D. M., Siepmann, J. I., Truhlar, D. G., Eds.; John Wiley & Sons: New York, 1999; Vol. 105, and references therein.

(51) Hase, W. L. Classical Trajectory Simulations: Initial Conditions. In *Encyclopedia of Computational Chemistry*; Schleyer, P. V. R., Allinger, N. L., Clark, T., Gasteiger, J., Kollman, P. A., Schaefer, H. F., III, Schreiner, P. R., Eds.; Wiley: New York, 1998.

(52) Andersen, A.; Carter, E. A. Unpublished work.
(53) Doubleday, C., Jr.; Bolton, K.; Peslherbe, G. H.; Hase, W. L. *J. Am. Chem. Soc.* **1996**, *118*, 9922.
(54) Schaftenaar, G.; Noordik, J. M. *J. Comput.-Aided Mol. Des* **2000**, *14*, 124−134.
(55) Flükiger, P.; Lüthi, H. P.; Portmann, S.; Weber, J. *MOLEKEL*, ver. 4.1; Swiss Center for Scientific Computing: Manno, Switzerland, 2000−2001.
(56) Knyazev, V. D.; Slagle, I. R. *J. Phys. Chem.* **1998**, *102*, 1770.
(57) Ellison, G. B. Private communications.
(58) Benson, S. W. *Thermochemical Kinetics*, 2nd ed.; John Wiley & Sons: New York, 1976; p 300.
(59) Herzberg, G. *Molecular Spectra and Molecular Structure. III. Electronic Spectra and Electronic Structure of Polyatomic Molecules*; Van Nostrand: New York, 1967.
(60) Ruiz, R. P.; Bayes, K. D. *J. Phys. Chem.* **1984**, *88*, 2592.
(61) Paltenghi, R.; Ogryzlo, E. A.; Bayes, K. D. *J. Phys. Chem.* **1984**, *88*, 2595.
(62) Xi, Z.; Han, W.-J.; Bayes, K. D. *J. Phys. Chem.* **1988**, *92*, 3450.
(63) Representative movies may be viewed at http://www.chem.ucla.edu/dept/Faculty/carter/movies.html.
(64) Pople, J.; Gill, P.; Handy, N. *Int. J. Quantum Chem.* **1995**, *56*, 303.
(65) Pushkarsky, M. B.; Zalyubovsky, S. J.; Miller, T. A. *J. Chem. Phys.* **2000**, *112*, 10695.
(66) Tuckett, R. P.; Freedman, P. A.; Jones, W. J. *Mol. Phys.* **1979**, *37*, 403.
(67) Hunziker, H. E.; Wendt, H. R. *J. Chem. Phys.* **1974**, *60*, 4622.
(68) Tuckett, R. P.; Freedman, P. A.; Jones, W. J. *Mol. Phys.* **1979**, *37*, 379.
(69) Fink, E. H.; Ramsay, D. A. *J. Mol. Spectrosc.* **1997**, *185*, 304.
(70) Ossman, G.; Bunker, P. R.; Jensen, P.; Buenker, R. J.; Gu, J.-P.; Hirsch, G. *J. Mol. Spectrosc.* **1999**, *185*, 304.
(71) Langhoff, S. R.; Jaffe, R. L. *J. Chem. Phys.* **1979**, *71*, 1475.
(72) Krishnan, R.; Binkley, J. S.; Seeger, R.; Pople, J. A. *J. Chem. Phys.* **1980**, *72*, 650.
(73) Howard, C. J. *J. Am. Chem. Soc.* **1980**, *102*, 6937.
(74) Gurvich, L. V.; Veyts, I. V.; Alcock, C. B.; Iorish, V. S. *Thermodynamic Properties of Individual Substances*, 4th ed.; Hemisphere: New York, 1991.
(75) Ramond, T. M.; Blanksby, S. J.; Kato, S.; Bierbaum, V. M.; Davico, G. E.; Schwartz, R. L.; Lineberger, W. C.; Ellison, G. B. Unpublished data.